5. Ritchie, M. G. & Phillips, S. D. F. in *Endless Forms: Species and Speciation* (eds Howard, D. J. & Berlocher, S. H.) 291–308 (Oxford Univ. Press, New York, 1998).
6. Albertson, R. C., Markert, J. A., Danley, P. D. & Kocher, T. D. Phylogeny of a rapidly evolving clade: The cichlid fishes of Lake Malawi, East Africa. *Proc. Natl Acad. Sci. USA* **96,** 5107–5110 (1999).
7. Tauber, C. A. & Tauber, M. J. in *Speciation and its Consequences* (eds Otte, D. & Endler, J. A.) 307–344 (Sinauer, Sunderland, 1989).
8. Bush, G. L. Sympatric speciation in animals: new wine in old bottles. *Trends Ecol. Evol.* **9,** 285–288 (1994).
9. Maynard Smith, J. Sympatric speciation. *Am. Nat.* **100,** 637–650 (1966).
10. Tauber, G. A. & Tauber, M. J. A genetic model for sympatric speciation through habitat diversification and seasonal isolation. *Nature* **268,** 702–705 (1977).
11. Doebeli, M. A quantitative genetic competition model for sympatric speciation. *J. Evol. Biol.* **9,** 893–909 (1996).
12. Kawecki, T. J. Sympatric speciation via habitat specialization driven by deleterious mutations. *Evolution* **51,** 1751–1763 (1997).
13. Kodrashov, A. S. & Kondrashov, F. A. Interactions among quantitative traits in the course of sympatric speciation. *Nature* **400,** 351–354 (1999).
14. Dieckmann, U. & Doebeli, M. On the origin of species by sympatric speciation. *Nature* **400,** 354–357 (1999).
15. Fisher, R. A. *The Genetical Theory of Natural Selection* (Clarendon, Oxford, 1930).
16. Lande, R. Models of speciation by sexual selection on polygenic traits. *Proc. Natl Acad. Sci. USA* **78,** 3721–3725 (1981).
17. Seger, J. Unifying genetic models for the evolution of female choice. *Evolution* **39,** 1185–1193 (1985).
18. Pomiankowski, A. The costs of choice in sexual selection. *J. Theor. Biol.* **128,** 195–218 (1987).
19. Liou, L. W. & Price, T. D. Speciation by reinforcement of premating isolation. *Evolution* **48,** 1451–1459 (1994).
20. Turner, G. F. & Burrows, M. T. A model of sympatric speciation by sexual selection. *Proc. R. Soc. Lond. B* **260,** 287–292 (1995).
21. Pomiankowski, A., Iwasa, Y. & Nee, S. The evolution of costly mate preferences I. Fisher and biased mutation. *Evolution* **45,** 1422–1430 (1991).
22. Iwasa, Y., Pomiankowski, A. & Nee, S. The evolution of costly mate preferences II. The 'handicap' principle. *Evolution* **45,** 1431–1442 (1991).
23. Wu, G.-I. A stochastic simulation study on speciation by sexual selection. *Evolution* **39,** 66–82 (1985).

Acknowledgements

M.H. thanks J. Lawton and the NERC Centre for Population Biology for their hospitality. This work was supported by a MESSC grant to M.H.

Correspondence and requests for materials should be addressed to M.H. (e-mail: higashi@ecology.kyoto-u.ac.jp).

Direct measurement of intra-cochlear pressure waves

Elizabeth S. Olson

Physics Department, Princeton University, Princeton, New Jersey 08544, USA

The cochlear travelling wave is fundamental to the ability of the mammalian auditory system to resolve frequency. The seashell-shaped outer bone of the cochlea (the auditory inner ear) contains a spiral of cochlear fluid and the sensory tissue known as the cochlear partition. Sound travels down the ear canal to the eardrum, causing its flexible tympanic membrane to vibrate. This vibration is transmitted to the cochlea via the ossicles. Motion of the stapes (the stirrup ossicle) sets the cochlear fluid in motion, which in turn sets the cochlear partition near the stapes in motion. The motion of the cochlear partition ripples down the cochlear spiral as a travelling wave, stimulating the cochlea's sensory hair cells. The wave peaks near the base (the stapes end) of the cochlea for high frequency tones and near the apex for low frequencies[1]. The fundamental elements of the cochlear travelling wave are fluid pressure and motion and partition forces and motion. However, the wave's direct experimental study has to date relied almost solely on measurements of the partition motion. Here I report finely spaced measurements of intracochlear pressure close to the partition, which reveal the fluid component of the cochlear wave. The penetration depth of the wave is very limited, ~15 μm. Over a range of frequencies at least an octave wide, the depth is independent of frequency.

I recently described pressure measurements made in the extreme base of the cochlea[2]; here a turn-one location, 14% further towards the apex along the cochlear spiral, is emphasized. Strong nonlinearity was detected at the turn-one location, whereas in the extreme base the responses were nearly linear, owing to the extreme fragility of that region. Therefore, the basal results describe the passive cochlea. Nonlinearity in the cochlea's mechanical response to sound is the key to its dynamic range and ability to finely separate frequencies. Outer hair cells appear to be essential to this mechanical enhancement[3,4], whereas the inner hair cells communicate information about the partition's motion to the auditory neurons[5].

Here I demonstrate the frequency and position dependence of the nonlinear fluid pressure. Pressure differences are used to find fluid velocity, and the results are interpreted with respect to the cochlear travelling wave. In particular, the wave's penetration depth is found to be ~15 μm. The penetration depth indicates how much fluid the wave contains, and its size and frequency dependence constrain cochlear models. In models, the fluid component of the cochlea is often simplified to one dimension—along the partition. In two-dimensional models the height of the fluid is included, and in three-

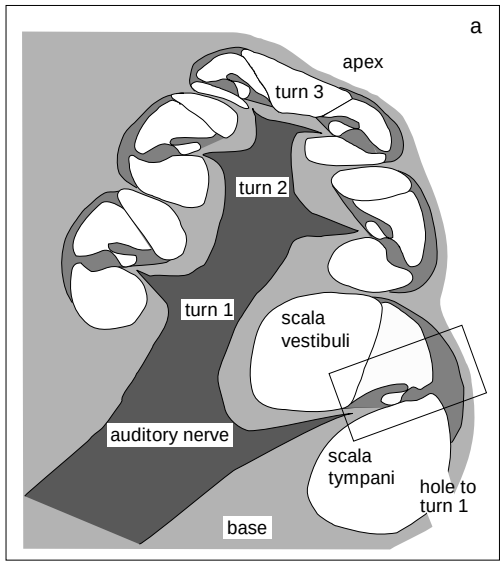

Figure 1 The cochlea. **a**, Cross-section of the gerbil cochlea; the boxed section is enlarged in **b**. The cochlear partition and the fluid compartments scala tympani and scala vestibuli spiral around the auditory nerve. The mongolian gerbil cochlea is ~2.6 mm in diameter, with a cochlear partition length of ~13 mm (ref. 16). In the extreme base of the cochlea the scala vestibuli is terminated by the stapes, the scala tympani by the round window membrane (not shown). The general location of a hand-drilled hole used to access turn one scala tympani is indicated in **a**. The scala tympani pressure sensor was positioned to approach the basilar membrane approximately perpendicularly. The sensor's outer diameter is 170 μm. (The drawings derive from a 2-mm plastic-embedded section prepared by M. Feldman.)

dimensional models the finite widths of the fluid compartments and cochlear partition are also used. The small, frequency-insensitive penetration depth emphasizes the significance of all three dimensions for modelling and understanding cochlear mechanics.

The measurements were made in deeply anaesthetized gerbils stimulated with tones via a speaker coupled to the ear canal. In each experiment one location along the cochlear spiral was probed in the scala tympani, either the extreme base or the first turn of the spiral (Fig. 1a). These basal and turn-one locations had characteristic frequencies of approximately 32 kHz and 20 kHz, consistent with Müller's place-frequency map of the gerbil cochlea[6]. The scala-tympani pressure measurements were made at a series of distances from the basilar membrane, a fibrous tissue that forms a boundary of the cochlear partition (Fig. 1b). The pressure in the scala vestibuli just next to the stapes was measured within seconds of each measurement in the scala tympani. This is the input pressure to the cochlea and served as a reference pressure. The results of one basal experiment and one turn-one experiment are shown in Figs 2–5, with the details of the basal experiment presented elsewhere[2].

Figure 2 shows turn-one scala-tympani pressure at the frequency of the stimulus, measured as the sensor approached the basilar membrane in 13 steps. For clarity, only five of the 13 curves are shown. The gain of the scala-tympani pressure relative to the pressure in the ear canal was as large as 50 dB. (For comparison, numerous experiments indicate that the gain of the scala-vestibuli pressure next to the stapes is ~30 dB and is almost flat at frequencies of 2–40 kHz (refs 2, 7).) At positions close to the basilar membrane the scala-tympani pressure peaked sharply at ~19 kHz when the stimulus level was 50 dB sound pressure level (SPL), and peaked broadly in the frequency band of 10–20 kHz when the stimulus level was 80 dB SPL. (50–60 dB SPL is a conversational sound level; 80 dB SPL is the level of an alarm clock two feet away.) The difference in the sharpness of tuning occurred because at frequencies in the vicinity of the characteristic frequency the response magnitude did not scale linearly with stimulus level, but was compressed. This type of cochlear nonlinearity is well known from measurements of basilar-membrane motion[8]. The nonlinearity depends on physiological processes, because after death the pressure scaled linearly with stimulus level. Close to the basilar membrane, the phase of the scala-tympani pressure relative to the scala-vestibuli pressure decreased smoothly through more than a complete cycle as the frequency varied from 10 to 23 kHz. This accumulating phase is expected for a travelling wave, and is similar to the phase of basilar-membrane motion[9]. The notches that appeared in the magnitude at frequencies in the vicinity of the characteristic frequency are believed to be caused by destructive interference between two modes of cochlear pressure[2]. One of the modes is coupled to the cochlear travelling wave. The phase of this mode goes through large excursions (referenced to the input pressure in the scala vestibuli) and its magnitude decreases with distance from the basilar membrane. The other mode is more closely tied to the stapes motion and its magnitude and phase are expected to vary in space relatively slowly[10]. In this interpretation, the substantial pressure at frequencies well above the characteristic frequency, where the phase accumulation ceased, was due to the non-travelling wave mode. The pressure peak was substantially smaller and the phase no longer accumulated smoothly at distances 100–300 μm from the basilar membrane. Spatial pressure variations indicate fluid motion, and the rapid decrease of pressure with distance demonstrates the localized nature of the travelling wave disturbance in the fluid. At frequencies above the characteristic frequency, although the pressure was large, pressure variations were very small—substantial fluid motions were only present with the travelling wave. To quantify the fluid motions, the velocity of the fluid in the direction perpendicular to the basilar membrane was found from the spatial pressure variations. Fluid velocity is important because the rapidity with which it falls off with distance from the basilar membrane gives the penetration depth of the travelling wave in the fluid. The direct use of pressure to find the penetration depth of the travelling wave is confounded by the large non-travelling pressure mode.

The calculation of the z-component of fluid velocity begins by taking the difference between two pressures from adjacent positions along the z-axis (Fig. 1b); for example, those measured 7 μm and 22 μm from the basilar membrane. This difference divided by the distance between the measurements approximates the z-component of the pressure gradient. The gradient is related to fluid velocity via the Navier-Stokes equation

$$\nabla P = -\rho \partial v/\partial t + -\rho v \cdot \nabla v + \mu \nabla^2 v \qquad (1)$$

where P is pressure, v is velocity, ∇ is the gradient operator, ∇^2 is the laplacian operator, and ρ and μ are the density and viscosity of the cochlear fluid. At frequencies above ~8 kHz, ∇P can be approximated using only the first term on the right-hand of this equation, and the velocity can be written very simply[2]. Here P_b and P_a are two pressures measured at positions adjacent to each other on the z-axis with P_a further from the basilar membrane, and v_z is the z-component of the velocity. The difference Δz is the distance between the pressure measurements. The time derivative is written as $i\omega$ where ω is angular frequency

$$v_z = (i/\omega)(P_a - P_b)/(\rho \Delta z) \qquad (2)$$

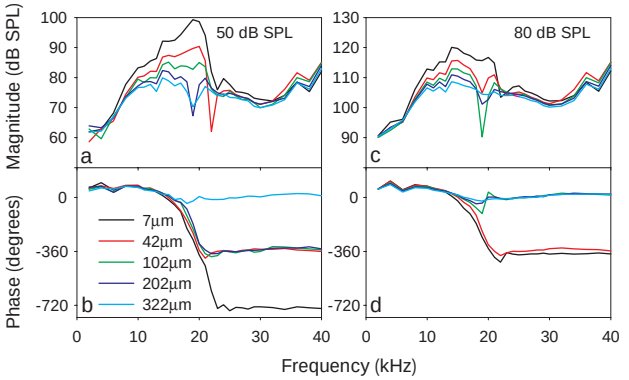

Figure 2 Scala tympani pressure versus frequency at the turn-one location. Each curve was measured at the distance from the b.m. indicated in the key. Pressure was also measured at 22, 62, 82, 122, 142, 162, 182, and 302 μm from the basilar membrane. **a**, **b**, Magnitude and phase, 50 dB SPL stimuli (as measured in ear canal); **c** and **d**, magnitude and phase, 80 dB SPL stimuli. Magnitude is expressed as SPL, defined as dB with respect to 20 μPa. The phase is referenced to the scala vestibuli pressure next to the stapes. (Scala tympani pressure with an accumulating phase such as that illustrated here has been measured in five basal and 13 turn-one experiments.)

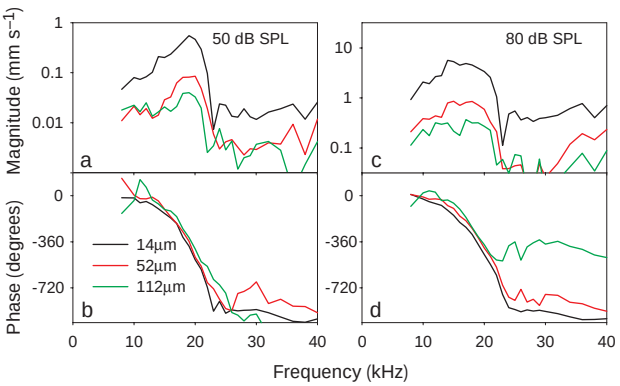

Figure 3 Fluid velocity derived from pressures of Fig. 2. Magnitude and phase of the derived velocity (z-component) are shown as a function of frequency at three distances from the basilar membrane. The phase is referenced to the scala vestibuli pressure next to the stapes. **a**, **b**, Magnitude and phase, 50 dB SPL stimuli; **c**, **d**, magnitude and phase, 80 dB SPL stimuli.

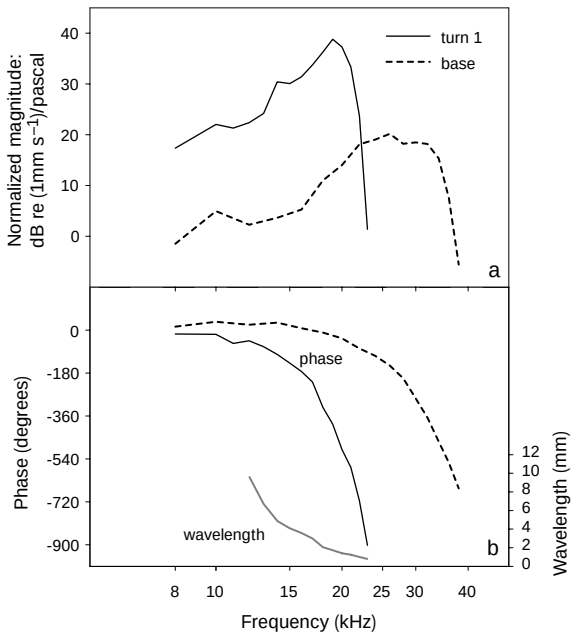

Figure 4 Fluid velocity (*z*-component) close to the basilar membrane at turn-one and basal locations, and wavelength of cochlear wave. **a**, **b**, Magnitude and phase. The magnitude is normalized to the stimulus level in the ear canal. The phase is referenced to the scala vestibuli pressure next to the stapes. Stimulus levels were 50 dB SPL (turn one) and 60 dB SPL (base). Inset in **b**, and using the right axis, is the wavelength of the cochlear travelling wave as a function of frequency. The derived wavelength corresponds to a location on the cochlear spiral that is midway between the basal and turn-one locations.

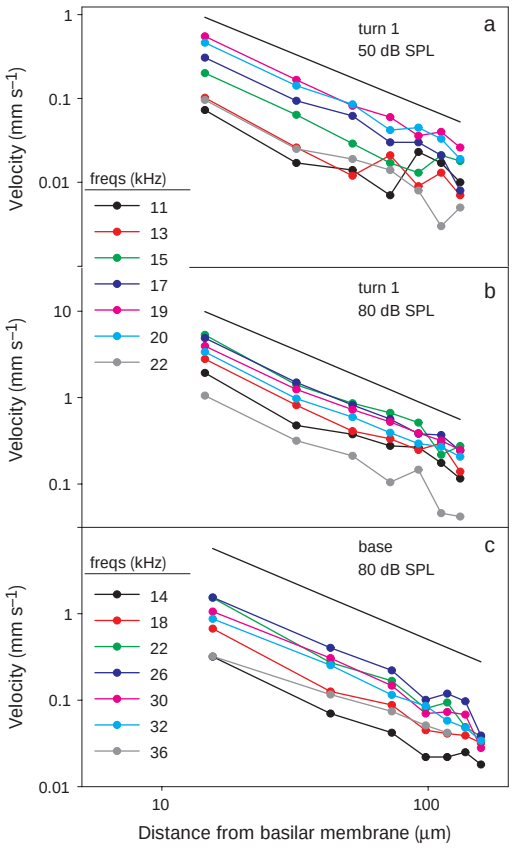

Figure 5 Fluid velocity (*z*-component) as a function of distance from the basilar membrane. **a**, Turn-one location, 50 dB SPL stimuli. **b**, Turn-one location, 80 dB SPL stimuli. **c**, Basal location, 80 dB SPL stimuli. The black line without data points is a power law with exponent −1.3. (The fall-off of fluid velocity with distance illustrated here has been repeated in the four additional turn-one experiments that were part of this study.)

Figure 3 shows v_z as a function of frequency and distance from the basilar membrane, calculated with pairs of pressure measurements from the experiment of Fig. 2. The velocity magnitude did not contain the frequency and distance dependent notches which were seen in the pressure magnitude and were attributed to destructive interference between travelling-wave and non-travelling-wave pressure modes. The reason for the contrast is simple. Fluid velocity is based on the pressure gradient: spatial pressure differences. Only the travelling-wave mode (rapidly varying spatially) contributes substantially to the gradient; the non-travelling mode (slowly varying spatially) cancels out the difference. This cancellation also caused the velocity phases to go through larger and smoother excursions compared to their pressure counterparts.

I also found the wavelength and penetration depth of the travelling wave. Figure 4 shows the fluid velocity close to the basilar membrane for the turn-one experiment of Figs 2 and 3, and for a basal experiment. The fluid very close to the basilar membrane is expected to move with it. Thus, these results estimate basilar-membrane velocity. The validity of this estimation is supported by the similarity between these results and those of direct measurements of basilar-membrane velocity from the literature[11,12]. It is possible to estimate the travelling wave wavelength from the phase data and the observation that the two locations (basal and turn one) were spaced by ~1.8 mm. Then $\lambda = 1.8(360/\Delta\phi)$, where λ is the wavelength in mm and $\Delta\phi$ is the phase difference between the two locations in degrees. This wavelength belongs to a location on the cochlear spiral that is midway between the basal and turn one locations, where the characteristic frequency would be ~25 kHz. Wavelength is plotted against frequency in Fig. 4. The wavelength decreased by a factor of ten as the frequency roughly doubled. This rapidly decreasing wavelength reflects the decreasing speed of the travelling wave as the stimulus frequency approached the characteristic frequency[10]. At 23 kHz, the wavelength is found to be just under 1 mm, which is similar to previously reported wavelengths near the characteristic frequency in the basal region of squirrel monkey[8], cat and guinea pig[13]. (The fact that the basal pressure behaved linearly is not expected to change the wavelength prediction greatly, because the response phase is relatively insensitive to stimulus level and cochlear condition (Fig. 3 and ref. 9).)

Figure 5 shows the magnitude of the velocity versus distance from the basilar membrane at frequencies from almost an octave below the characteristic frequency to just above it. The reduction in velocity with distance was smooth and rapid. It was quite insensitive to frequency, stimulus level and location along the spiral. (Less than 30 μm from the basilar membrane, the fluid velocity increased with distance in some experiments. These short-range disturbances are the subject of further study.) Included in the velocity–distance graphs is a line representing a power law with exponent −1.3. The penetration depth, δ, is defined as the distance from the closest velocity measurement to the place where the velocity is reduced by a factor of e. From the power law, $\delta = 15$ μm, a distance less than one-tenth the width of the cochlear partition and smaller than the length of a hair cell.

The insensitivity of the penetration depth to frequency is remarkable, particularly when interpreted with respect to cochlear models. As in an ocean wave, the penetration depth is expected to depend on wavelength and, as Fig. 4 makes clear, the wavelength is sensitive to frequency. However, the width of the partition, ~200 μm, is smaller than even the smallest wavelength. The results here suggest that it is this dimension that governs the penetration depth, and intuitively, it is reasonable that the smaller dimension should rule. More rigorously, a quantity from cochlear modelling that is related to the penetration depth is the 'effective mass' of the fluid. In one- and

two-dimensional models, the effective mass falls steeply as wavelength decreases. In three-dimensional models, in a fairly broad frequency range near the response peak, the effective mass becomes substantially less sensitive to wavelength[14,15]. In light of this behaviour, and the intuitive argument above, the observed lack of frequency sensitivity in the penetration depth does not seem all that surprising. □

Methods

Pressure sensor

A sensor consists of a glass capillary (inner and outer diameters 100 and 170 μm, respectively) tipped with a gold-coated polymer diaphragm. Light from an LED is delivered via a fibre optic threaded into the capillary, and reflects from the diaphragm. The amount of light returning to the fibre optic for transmission to a photodetector varies linearly with the pressure-induced bending of the diaphragm. The acoustic impedance of the sensors is an order of magnitude larger than that of the cochlea, and their presence does not 'load' the cochlea outright. Nevertheless, in some animals small reversible changes in compound action potential (CAP) threshold and/or scala vestibuli pressure occurred when the scala tympani sensor was close to the basilar membrane. However, the derived fluid velocity close to the basilar membrane was similar to that measured directly by others[11,12], suggesting that the sensor's presence does not cause large changes in cochlear mechanics.

Experimental procedure

Animal procedures were approved by the Princeton University IACUC. The experimental animals were young adult gerbils. A gerbil was deeply anaesthetized and its left cochlea was exposed. Tones from a loudspeaker were delivered to the ear via a tube fitted to the left ear canal. The level of the tones was calibrated in the ear canal at the beginning of each experiment. Basal scala tympani pressure measurements were made by inserting a pressure sensor through the round window opening after removing the covering membrane. Scala vestibuli and turn-one scala tympani measurements were made through small holes hand-drilled in the cochlear bone. In basal experiments it was possible to see the basilar membrane in order to position the scala tympani sensor. In turn-one experiments it was positioned by using anatomical landmarks and referring to widely opened excised cochleae. It was not practical to systematically check the precision of positioning in each experiment. However, the grouped data indicate that incorrectly positioning the sensor towards the spiral ligament caused substantial damage, and that incorrectly positioning the sensor over the spiral lamina caused greatly diminished pressure gradients. The distance between the basilar membrane and the sensor was determined by touching the former with the latter, which produced a characteristically noisy signal.

Stimulus generation and recording was performed with a Tucker Davis Technologies DA/AD system. With typical signal averaging times of 3 s, sound pressure above the level of 60–70 dB SPL (20–60 mPa) could be reliably measured.

As a gauge of cochlear health, an electrode at the round window measured the CAP response of the auditory nerve to tones. The CAP threshold is the minimum sound level required to elicit a reliable neural response. Initial thresholds in the turn one experiment were ≤30 dB SPL at 15 and 20 kHz, and 50 dB SPL at 25 kHz. Close to the time of measurements, these thresholds were 40, 40, and 50–60 dB SPL. Initial thresholds in the basal experiment were ≤60 dB SPL at 30 kHz, and 80 dB SPL at 40 kHz. Close to the time of measurements, they were 60 and >80 dB SPL. At the frequencies of interest, the initial CAP thresholds in the turn one experiment were in keeping with those of Müller[6], those in the basal experiment were elevated somewhat. The degree of nonlinearity observed in the scala tympani pressures was consistent with the health of the cochlea as indicated by the CAP threshold—the basal experiment was nearly linear, and the nonlinearity in the turn-one experiment was strong, but not among the strongest in the literature[9].

Received 1 June; accepted 4 October 1999.

1. von Bekesy, G. *Experiments in Hearing* (McGraw Hill, New York, 1960).
2. Olson, E. S. Observing middle and inner ear mechanics with novel intracochlear pressure sensors. *J. Acoust. Soc. Am.* **103,** 3445–3463 (1998).
3. Brownell, W. E., Bader, C. R., Betrand, D. & de Ribaupierre, Y. Evoked mechanical responses of isolated cochlear outer hair cells. *Science* **227,** 195–196 (1985).
4. Liberman, M. C. & Dodds, L. W. Single neuron labeling and chronic cochlear pathology. III. Stereocilia damage and alterations of threshold tuning curves. *Hear. Res.* **16,** 55–74 (1984).
5. Spoendlin, H. Innervation densities of the cochlea. *Acta Otolaryngol. (Stockh.)* **73,** 235–248 (1972).
6. Müller, M. The cochlear place-frequency map of the adult and developing mongolian gerbil. *Hear. Res.* **94,** 148–156 (1996).
7. Dancer, A. & Franke, R. Intracochlear sound pressure measurements in guinea pigs. *Hear. Res.* **2,** 191–205 (1980).
8. Rhode, W. S. Observations of the vibration of the basilar membrane in squirrel monkeys using the Mossbauer Technique. *J. Acoust. Soc. Am.* **49,** 1218–1231 (1971).
9. Ruggero, M., Rich, N. C., Recio, A., Narayan, S. S. & Robles, L. Basilar membrane responses to tones at the base of the chinchilla cochlea. *J. Acoust. Soc. Am.* **101,** 2151–2163 (1997).
10. Lighthill, J. Energy flow in the cochlea. *J. Fluid Mech.* **106,** 149–213 (1981).
11. Sellick, P. M., Yates, G. K. & Patuzzi, R. The influence of Mossbauer source size and position on phase and amplitude measurements of the guinea pig basilar membrane. *Hear. Res.* **10,** 101–108 (1983).
12. Xue, S., Mountain, D. C. & Hubbard, A. E. Electrically evoked basilar membrane motion. *J. Acoust. Soc. Am.* **97,** 3030–3041 (1995).
13. Cooper, N. P. & Rhode, W. S. Basilar membrane mechanics in the hook region of cat and guinea-pig cochlea: Sharp tuning and nonlinearity in the absence of baseline position shifts. *Hear. Res.* **63,** 163–190 (1992).
14. de Boer, E. Auditory physics. Physical principles in hearing theory. II. *Phys. Rep.* **105,** 141–226 (1984).
15. Steele, C. R. & Taber, L. A. Comparison of WKB calculations and experimental results for three-dimensional cochlear models. *J. Acoust. Soc. Am.* **65,** 1007–1018 (1979).
16. Plassman, W., Peetz, W. & Schmidt, M. The cochlea in gerbilline rodents. *Brain Behav. Evol.* **30,** 82–101 (1987).

Acknowledgements

I thank H. Nakajima, E. de Boer, L. Sohn, N. Cooper, S. Staggs, R. Brawer, R. Austin and L. Page Jr. This work was supported by the National Institute on Deafness and Other Communication Disorders.

Correspondence and requests for materials should be addressed to E.O. (e-mail: eolson@princeton.edu).

Stable propagation of synchronous spiking in cortical neural networks

Markus Diesmann*, Marc-Oliver Gewaltig* & Ad Aertsen

Department of Neurobiology and Biophysics, Institute of Biology III, Albert-Ludwigs-University, Schänzlestraße 1, D-79104 Freiburg, Germany

The classical view of neural coding has emphasized the importance of information carried by the rate at which neurons discharge action potentials. More recent proposals that information may be carried by precise spike timing[1–5] have been challenged by the assumption that these neurons operate in a noisy fashion—presumably reflecting fluctuations in synaptic input[6]—and, thus, incapable of transmitting signals with millisecond fidelity. Here we show that precisely synchronized action potentials can propagate within a model of cortical network activity that recapitulates many of the features of biological systems. An attractor, yielding a stable spiking precision in the (sub)millisecond range, governs the dynamics of synchronization. Our results indicate that a combinatorial neural code, based on rapid associations of groups of neurons co-ordinating their activity at the single spike level, is possible within a cortical-like network.

Evidence is accumulating that cortical neurons *in vivo* are capable of producing action potentials with high temporal accuracy. In recordings of multiple single-neuron activity in behaving monkeys, precisely timed action potentials have been systematically related to stimuli and behavioural events, indicating that these instances of precise spike timing play a functional role[1–3]. Independent evidence for precise spike timing in cortical neurons came from intracellular recordings *in vitro*[4,5]. But can an instance of synchronous spiking, once it has occurred, be successfully propagated by subsequent groups of cortical neurons? Under which input conditions can a group of cortical neurons engage in precisely coordinated spike timing, and are such conditions feasible in the cortical network? How can we clarify and quantify the notions of 'well timed' and 'reliable', which gained such a prominent role in the on-going debate on temporal coding in the brain?[7–10] Clearly, these questions must be resolved to determine whether cortical computation on the basis of precise spike timing is possible. Preliminary results have been presented in abstract form[11,12].

To address these questions, we have studied the fine-grained temporal response properties of the 'integrate-and-fire' neuron, a widely used class of model neurons capturing essential properties of

* Present addresses: Department of Nonlinear Dynamics, Max-Planck-Institut für Stömungsforschung, Göttingen, Germany (M.D.); Future Technology Research, Honda R&D Europe, Offenbach, Germany (M.-O.G.)